JACS
JOURNAL OF THE AMERICAN CHEMICAL SOCIETY
Communication
pubs.acs.org/JACS

CO_2 Dynamics in a Metal–Organic Framework with Open Metal Sites

Xueqian Kong,*[,†,§] Eric Scott,[‡] Wen Ding,[†] Jarad A. Mason,[‡] Jeffrey R. Long,[‡,∥] and Jeffrey A. Reimer[†,§]

[†]Department of Chemical and Biomolecular Engineering and [‡]Department of Chemistry, University of California Berkeley, Berkeley, California 94720, United States

[§]Environmental Energy Technologies Division and [∥]Materials Sciences Division, Lawrence Berkeley National Laboratory, Berkeley, California 94720, United States

Supporting Information

ABSTRACT: Metal–organic frameworks (MOFs) with open metal sites are promising candidates for CO_2 capture from dry flue gas. We applied *in situ* ^{13}C NMR spectroscopy to investigate CO_2 adsorbed in Mg_2(dobdc) (H_4dobdc = 2,5-dihydroxyterephthalic acid; Mg-MOF-74, CPO-27-Mg), a key MOF in which exposed Mg^{2+} cation sites give rise to exceptional CO_2 capture properties. Analysis of the resulting spectra reveals details of the binding and CO_2 rotational motion within the material. The dynamics of the motional processes are evaluated via analysis of the NMR line shapes and relaxation times observed between 12 and 400 K. These results form stringent and quantifiable metrics for computer simulations that seek to screen and improve the design of new MOFs for CO_2 capture.

The continued use of fossil fuels generates considerable challenges for the capture and sequestration of the greenhouse gas CO_2. Among various possibilities (amine scrubbing, zeolites, porous membranes, etc.), metal–organic frameworks (MOFs) represent one of the most promising candidates for CO_2 capture from flue gases.[1−5] Fundamental molecular-level knowledge regarding CO_2 adsorption dynamics in MOFs, however, remains sparse and has impeded the systematic molecular design of these materials. Furthermore, a detailed understanding of the binding and dynamics of CO_2 in MOFs is necessary to validate and refine computer simulations[6−8] that seek to accurately assess these materials for CO_2 adsorption selectivity and process compatibility.

MOFs with open metal sites, such as M_2(dobdc) (M = Mg, Ni, Co, Mn, Fe, Zn; H_4dobdc = 2,5-dihydroxyterephthalic acid) have greatly improved adsorption and selectivity for CO_2 gas.[9−14] The structure of activated Mg_2(dobdc) (Mg-MOF-74, CPO-27-Mg) consists of an array of 1.1 nm-wide one-dimensional hexagonal channels with Mg^{2+} ions bearing an open coordination site at the vertices.[15−17] The exposed Mg^{2+} ions are known to act as the preferential adsorption sites for CO_2 according to density function theory (DFT) calculations[18−22] and as evidenced by neutron powder diffraction experiments,[19,23] as well as by infrared and Raman spectroscopy.[18,20] However, studies on the dynamics of adsorbed CO_2 over a temperature range relevant to CO_2 capture applications remains elusive. To fill this gap, we performed *in situ* ^{13}C NMR measurements of CO_2 adsorbed in Mg_2(dobdc) from the low temperature of 12 K up to 400 K, revealing a detailed picture of the dynamics of CO_2 rotational motion in Mg_2(dobdc).

The compound Mg_2(dobdc) was synthesized and activated using a strategy adopted from previous reports.[16,17] Here, $Mg(NO_3)_2{\cdot}6H_2O$ and H_4dobdc were allowed to react in *N*,*N*-dimethylformamide (DMF) at 120 °C. The resulting microcrystalline powder was washed repeatedly with DMF and methanol, and then dried under vacuum at 453 K. The successful synthesis and activation of the framework was confirmed by comparing the X-ray powder diffraction pattern, infrared spectrum, and Langmuir surface area to previously reported results.

NMR experiments began with the introduction of ^{13}C-enriched CO_2 into Mg_2(dobdc) by cryo-pumping into an evacuated Mg_2(dobdc) sample, which was subsequently flame-sealed in a glass tube. Static, variable-temperature ^{13}C NMR measurements were performed at 7.05 T magnets using either a commercial or a home-built NMR probe[24] with Tecmag NMR instruments. In these experiments, the ^{13}C signal from the MOF matrix was found to be negligible due to the low density of ^{13}C spins at natural abundance. Figure 1 shows the resulting ^{13}C NMR spectra of CO_2 adsorbed in Mg_2(dobdc) for two CO_2 loadings: 0.3 and 0.5 CO_2/Mg^{2+}, as determined based upon calibrated ^{13}C signal intensities at 298 K.

In the temperature range from 200 to 380 K, the ^{13}C lineshapes exhibit a distinct chemical shift anisotropy (CSA) powder pattern. This pattern comes from the orientation-dependent NMR chemical shift frequencies of a collection of detected nuclear spins. The ^{13}C spectra in Figure 1 provide direct evidence of a strong physical interaction between CO_2 and the MOF matrix, as the motional freedom of CO_2 has been dramatically reduced. Moreover, the line shape cannot be explained merely as a result of the spatial confinement of CO_2 in the nanometer-sized pores. On the basis of the axial symmetric narrowing of CO_2 CSA tensors, the powder patterns are best interpreted as the result of uniaxial rotation with a fixed rotation angle θ, as illustrated in Figure 2. This interpretation is consistent with previous studies, which all indicate that CO_2 molecules bind to Mg^{2+} sites with an end-on coordination.[18−20,23,25] It is reasonable to assume that the geometric center of the rotation axis is along the Mg–O(CO_2) vector, although it is not uniquely defined by the NMR data. This

Received: July 12, 2012
Published: August 21, 2012

   dx.doi.org/10.1021/ja306822p | *J. Am. Chem. Soc.* 2012, 134, 14341−14344

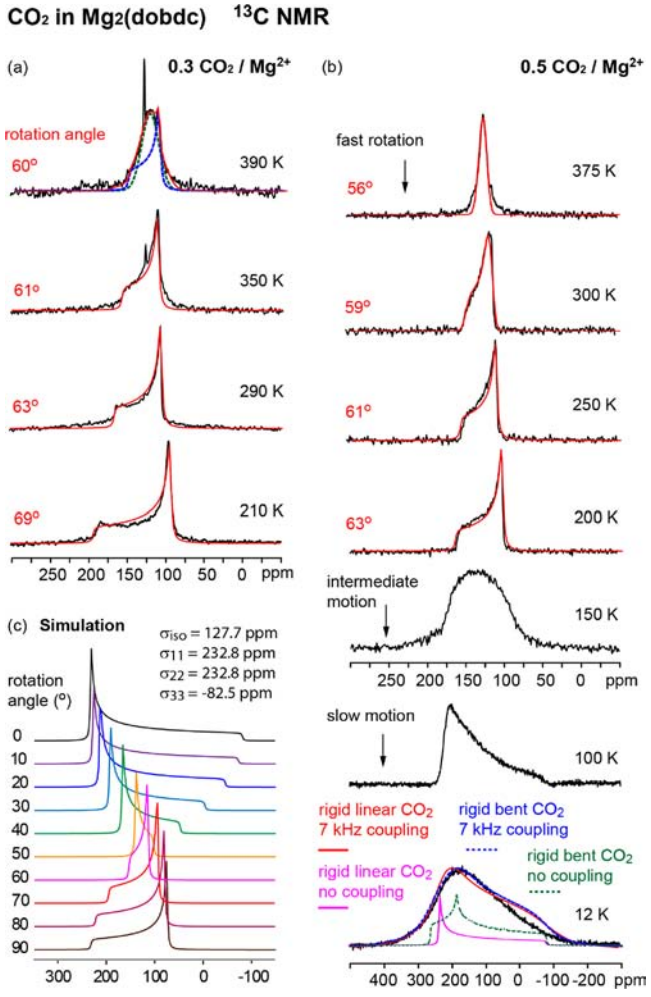

Figure 1. ^{13}C CSA powder patterns of ^{13}C-enriched CO_2 in $Mg_2(dobdc)$ at various temperatures. The colored lines are from line shape simulations of uniaxial rotation of CO_2 at a fixed rotation angle θ: (a) ^{13}C lineshapes of the 0.3 CO_2/Mg sample, (b) ^{13}C lineshapes of the 0.5 CO_2/Mg sample, and (c) ^{13}C lineshapes from simulations of CO_2 uniaxial rotation. The estimated errors for the rotation angles reported in (a) and (b) are within ±0.3°.

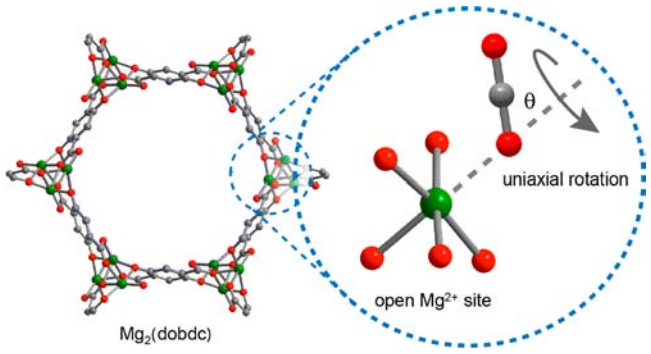

Figure 2. Schematic illustration of CO_2 uniaxial rotation at the open Mg^{2+} site in $Mg_2(dobdc)$. Gray, red, and green spheres represent C, O, and Mg atoms, respectively; H atoms are omitted for clarity. Note that the rotation axis is arbitrarily drawn in the picture.

mode of rotation has been observed for CO_2 confined in activated carbon fibers and CO_2 clathrate hydrates.[26,27]

Motional averaged NMR line shapes can be simulated by a number of computer packages, including the Internet-accessible program NMR-WEBLAB[28] used in this paper. We assumed a linear geometry for the CO_2 molecules with the CSA tensors $\sigma_{11} = \sigma_{22} = 232$ ppm, $\sigma_{33} = -82.5$ ppm.[29] The simulation was performed under the fast motion limit (i.e., assuming the rotation rate exceeds 1×10^6 Hz) with 6-site jumps of equal populations (i.e., a rotation with 6 discrete steps), which gives equivalent patterns as uniaxial rotation. Note that, under the fast motion limit, the CO_2 CSA patterns are equivalent for axially symmetric N-site jumps ($N \geq 3$), but not for 2-site jumps or other nonaxially symmetric motions. A bent geometry for the CO_2 molecule when adsorbed has been suggested by DFT calculations and neutron powder diffraction, although the exact C−O−C angle remains a matter of debate.[19−23] Nevertheless, inclusion of a bent CO_2 molecule in our simulation does not qualitatively alter our NMR results in the fast motional regime.

According to our simulations, the CO_2 rotation angle θ varies in a range from 56° to 69°, depending upon the temperature and the degree of loading. The NMR-derived angles agree qualitatively with the range of approximately 51−59° calculated under a rigid condition using DFT,[18,20] as well as with the angle of 52−55° determined by neutron powder diffraction at 20 K.[23] We note that simulations in the fast motional regime based upon a bent CO_2 with C−O−C angle of 160° also match the NMR data if the above-mentioned angles are decreased by around 5°. For both loadings measured, the CO_2 rotation angle increases as the temperature is lowered; however, the angles obtained for the lower loading are slightly greater than those obtained for the higher loading at the same temperatures. For example, at 300 K, the rotation angle is 63° for 0.3 CO_2/Mg^{2+} compared to 59° for 0.5 CO_2/Mg^{2+}.

At temperatures above 340 K, a ^{13}C resonance associated with gaseous CO_2, corresponding to a sharp peak at ∼125 ppm, is observed for the 0.3 CO_2/Mg^{2+} sample (see the top two spectra in Figure 1a). In contrast, no such peak is seen for the 0.5 CO_2/Mg^{2+} sample at high temperatures. This is due to the relative amount of gaseous CO_2 compared to adsorbed CO_2 in each sample tube. In the 0.3 CO_2/Mg^{2+} sample, a significant portion (∼40%) of adsorbed CO_2 has to be released to maintain the partial pressure because of the longer NMR tube used (∼1500 mm^3 in volume). For the 0.5 CO_2/Mg^{2+} sample, the NMR tube had to be shortened (∼100 mm^3 in volume) in order to fit into the sample space of the cryostat. As a result, only ∼5% of the CO_2 is released to maintain the partial pressure in the 0.5 CO_2/Mg^{2+} sample. The CO_2 partial pressure for the two CO_2 loadings was extracted from the NMR signal intensities of adsorbed CO_2, based upon the experimental gas adsorption isotherms reported previously (see Figure S3).[10] In these two samples, the CO_2 partial pressure increases from ∼0.01 bar at 300 K to ∼0.7 bar at around 400 K.

Interestingly, two populations of adsorbed CO_2 are observed at temperatures above 390 K in the 0.3 CO_2/Mg^{2+} sample, as shown in the top spectrum of Figure 1a. One population maintains the CSA powder pattern of uniaxial rotation at a fixed angle of 60° (blue dashed curve), while the other adopts a Gaussian-like line shape with a full-width-at-half-maximum of ∼1500 Hz (green dashed curve). This line shape is consistent with CO_2 rotation at variable angles of approximately 50−65°. The ratio of these two populations (blue versus green) is roughly 5:2. Random reorientation of CO_2 molecules, however, would yield a much narrower line shape. This second population could possibly correspond to a second adsorption site, as suggested previously,[23] although in those studies the

dx.doi.org/10.1021/ja306822p | J. Am. Chem. Soc. 2012, 134, 14341−14344

second site is only occupied at CO_2 loadings higher than 1.0 CO_2/Mg^{2+}. For the 0.5 CO_2/Mg^{2+} sample, Gaussian broadening of ~750 Hz has to be added to the CSA patterns for rotations at a fixed angle in order to match the ^{13}C line shape at temperatures above 300 K. This observation can be explained as a relatively narrow distribution of the rotation angle θ.

Low temperature (10−200 K) experiments were performed on the 0.5 CO_2/Mg^{2+} sample using a continuous flow cryostat (see the lower spectra in Figure 1b). As the temperature decreases, CO_2 continues its rotational motion down to 150 K and below. At 150 K, the rate of rotation slows to the intermediate motional regime, which leads to a hump-like pattern. When the temperature is decreased to 100 K, the whole pattern flips and broadens, and starts to resemble the line shape of rigid CO_2, although the pattern is still modulated by residual rotation or liberational motion.[27] As the motion further decreases approaching 12 K, the pattern is further broadened by a $^{13}C-^{1}H$ dipolar coupling of ~7 kHz (red solid curve), which is consistent with the relaxation time analysis discussed below. With the strong broadening effect, the distinction between the pattern of linear CO_2 (red solid curve) and that of a bent CO_2 (blue dashed curve) is not significant. For comparison, we also show the rigid patterns without dipolar broadening for both geometries (pink solid curve for the linear geometry and green dashed curve for the bent geometry). Note that the CSA tensors of a bent CO_2 (σ_{11} = 268.7 ppm, σ_{22} = 190.7 ppm, σ_{33} = −76.3 ppm) were derived from the values of undistorted ones via simple geometric manipulations and a conserved σ_{iso}.

The correlation time and activation energy of the CO_2 rotation can be extrapolated from the ^{13}C spin−lattice (T_1) relaxation times based on Bloembergen-Purcell-Pound (BPP) theory. The experimental data were fit with spectral density functions with two contributions: one from fluctuating fields associated with the ^{13}C CSA and the other with fluctuating fields from $^{1}H-^{13}C$ dipolar couplings.[30,31] In this analysis, however, the $^{1}H-^{13}C$ dipolar coupling was found to be the primary relaxation source. The temperature dependence of the correlation time τ_c of rotation is assumed to obey the Arrhenius equation, $\tau_c^{-1} = \tau_0^{-1} \exp(-E_a/RT)$ where τ_0 is pre-exponential factor, E_a is activation energy, R is the gas constant and T is temperature in Kelvin. The resulting activation energy E_a, pre-exponential factor τ_0, and $^{1}H-^{13}C$ dipolar coupling strength $d_{1H\text{-}13C}$ are listed in Table 1. We did not attempt to fit the T_1 values measured below 100 K, since CO_2 rotational motion generally stops at these temperatures.

As shown in Figure 3, the Arrhenius plot of the relaxation data reveals that two different activated processes (and correlation times) are needed to account for all of the NMR data in the temperature range from 100 to 400 K. The higher activation energy process dominates at higher temperatures in both samples. In the 0.3 CO_2/Mg^{2+} sample, the temperature at which we observe a change in activation energy coincides with the onset of gaseous CO_2 release, as seen from changes in the NMR signal intensity. In the 0.5 CO_2/Mg^{2+} sample, the temperature at which the activation energy changes correlates with the noticeable line shape change from a single angle rotation to a rotation with slight angle variations (i.e., the nonideal CSA lineshapes at temperatures above 300 K). The activation energy for rotation is relatively lower in the sample with the greater CO_2 loading, suggesting that the Mg^{2+}-CO_2 binding gets weaker as loading increases.

Table 1. Dynamics Parameters for CO_2 Rotation in Mg_2(dobdc)

0.3 CO_2/Mg^{2+}			0.5 CO_2/Mg^{2+}		
E_a (kJ/mol)	τ_0 (s)	$d_{1H\text{-}13C}$ (kHz)	E_a (kJ/mol)	τ_0 (s)	$d_{1H\text{-}13C}$ (kHz)
	300−400 K			250−380 K	
10.0(2)[a]	5.0×10^{-12}	13.0	6.0(5)	1.0×10^{-11}	16.0
	220−300 K			150−250 K	
4.0(3)	1.3×10^{-10}	9.0	3.5(3)	2.0×10^{-10}	6.7

[a]The values in parentheses are the errors of fit.

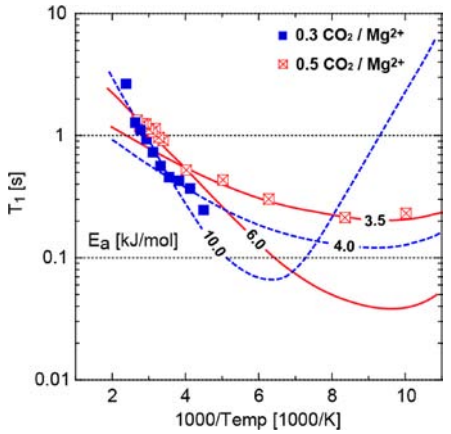

Figure 3. ^{13}C spin−lattice relaxation time (T_1) at various temperatures. The solid red curves show fits to the 0.5 CO_2/Mg^{2+} sample using the BPP methods described in the text, while the dashed blue curves show fits to the 0.3 CO_2/Mg^{2+} sample.

In summary, we investigated the motional dynamics of CO_2 adsorbed in Mg_2(dobdc) through ^{13}C NMR line shape and spin−lattice relaxation. These data were analyzed in the context of CO_2 uniaxial rotation at a relatively fixed angle over a broad temperature range (150−400 K). Activation energies and correlation times for the rotational motion have been derived from a BPP analysis of relaxation times. These results provide very stringent constraints for DFT and molecular dynamics simulations of CO_2 adsorption and motion that seek to improve the design of materials possessing open metal sites for carbon capture.

■ ASSOCIATED CONTENT

Ⓢ Supporting Information

Sample preparation, powder X-ray diffraction data, gas adsorption isotherms, details of NMR measurements and relaxation analysis. This material is available free of charge via the Internet at http://pubs.acs.org.

■ AUTHOR INFORMATION

Corresponding Author

xkong@lbl.gov

Notes

The authors declare no competing financial interest.

■ ACKNOWLEDGMENTS

This research was funded through the Center for Gas Separations Relevant to Clean Energy Technologies, an Energy Frontier Research Center funded by the US Department of Energy, Office of Science, Office of Basic Energy Sciences

under Award No. DE-SC0001015. We also thank NSF for providing graduate fellowship support (J.A.M.).

REFERENCES

(1) D'Alessandro, D. M.; Smit, B.; Long, J. R. *Angew. Chem., Int. Ed.* **2010**, *49*, 6058.
(2) Li, J. R.; Kuppler, R. J.; Zhou, H. C. *Chem. Soc. Rev.* **2009**, *38*, 1477.
(3) Rowsell, J. L. C.; Yaghi, O. M. *Microporous Mesoporous Mater.* **2004**, *73*, 3.
(4) Wang, Q. A.; Luo, J. Z.; Zhong, Z. Y.; Borgna, A. *Energy Environ. Sci.* **2011**, *4*, 42.
(5) Figueroa, J. D.; Fout, T.; Plasynski, S.; McIlvried, H.; Srivastava, R. D. *Int. J. Greenhouse Gas Control* **2008**, *2*, 9.
(6) Liu, B.; Smit, B. *Langmuir* **2009**, *25*, 5918.
(7) Yazaydin, A. O.; Snurr, R. Q.; Park, T. H.; Koh, K.; Liu, J.; LeVan, M. D.; Benin, A. I.; Jakubczak, P.; Lanuza, M.; Galloway, D. B.; Low, J. J.; Willis, R. R. *J. Am. Chem. Soc.* **2009**, *131*, 18198.
(8) Wilmer, C. E.; Leaf, M.; Lee, C. Y.; Farha, O. K.; Hauser, B. G.; Hupp, J. T.; Snurr, R. Q. *Nat. Chem.* **2012**, *4*, 83.
(9) Millward, A. R.; Yaghi, O. M. *J. Am. Chem. Soc.* **2005**, *127*, 17998.
(10) Mason, J. A.; Sumida, K.; Herm, Z. R.; Krishna, R.; Long, J. R. *Energy Environ. Sci.* **2011**, *4*, 3030.
(11) Bloch, E. D.; Queen, W. L.; Krishna, R.; Zadrozny, J. M.; Brown, C. M.; Long, J. R. *Science* **2012**, *335*, 1606.
(12) Deng, H. X.; Grunder, S.; Cordova, K. E.; Valente, C.; Furukawa, H.; Hmadeh, M.; Gandara, F.; Whalley, A. C.; Liu, Z.; Asahina, S.; Kazumori, H.; O'Keeffe, M.; Terasaki, O.; Stoddart, J. F.; Yaghi, O. M. *Science* **2012**, *336*, 1018.
(13) Sumida, K.; Rogow, D. L.; Mason, J. A.; McDonald, T. M.; Bloch, E. D.; Herm, Z. R.; Bae, T. H.; Long, J. R. *Chem. Rev.* **2012**, *112*, 724.
(14) Herm, Z. R.; Krishna, R.; Long, J. R. *Microporous Mesoporous Mater.* **2012**, *151*, 481.
(15) Dietzel, P. D. C.; Johnsen, R. E.; Blom, R.; Fjellvag, H. *Chem.—Eur. J.* **2008**, *14*, 2389.
(16) Britt, D.; Furukawa, H.; Wang, B.; Glover, T. G.; Yaghi, O. M. *Proc. Natl. Acad. Sci. U.S.A.* **2009**, *106*, 20637.
(17) Caskey, S. R.; Wong-Foy, A. G.; Matzger, A. J. *J. Am. Chem. Soc.* **2008**, *130*, 10870.
(18) Valenzano, L.; Civalleri, B.; Chavan, S.; Palomino, G. T.; Arean, C. O.; Bordiga, S. *J. Phys. Chem. C* **2010**, *114*, 11185.
(19) Wu, H.; Simmons, J. M.; Srinivas, G.; Zhou, W.; Yildirim, T. *J. Phys. Chem. Lett.* **2010**, *1*, 1946.
(20) Yao, Y. P.; Nijem, N.; Li, J.; Chabal, Y. J.; Langreth, D. C.; Thonhauser, T. *Phys. Rev. B* **2012**, 85.
(21) Poloni, R.; Smit, B.; Neaton, J. B. *J. Phys. Chem. A* **2012**, *116*, 4957.
(22) Dzubak, A.; Lin, L.-C.; Kim, J.; Swisher, J. A.; Poloni, R.; Maximoff, S. N.; Smit, B.; Gagliardi, L. *Nat. Chem.* **2012**, DOI: 10.1038/nchem.1432.
(23) Queen, W. L.; Brown, C. M.; Britt, D. K.; Zajdel, P.; Hudson, M. R.; Yaghi, O. M. *J. Phys. Chem. C* **2011**, *115*, 24915.
(24) Scott, E.; Stettler, J.; Reimer, J. A. *J. Magn. Reson.* **2012**, *221*, 117.
(25) Dietzel, P. D. C.; Johnsen, R. E.; Fjellvag, H.; Bordiga, S.; Groppo, E.; Chavan, S.; Blom, R. *Chem. Commun.* **2008**, 5125.
(26) Omi, H.; Ueda, T.; Miyakubo, K.; Eguchi, T. *Appl. Surf. Sci.* **2005**, *252*, 660.
(27) Ratcliffe, C. I.; Ripmeester, J. A. *J. Phys. Chem.* **1986**, *90*, 1259.
(28) Macho, V.; Brombacher, L.; Spiess, H. W. *Appl. Magn. Reson.* **2001**, *20*, 405.
(29) Bowers, C. R.; Long, H. W.; Pietrass, T.; Gaede, H. C.; Pines, A. *Chem. Phys. Lett.* **1993**, *205*, 168.
(30) Bloembergen, N.; Purcell, E. M.; Pound, R. V. *Phys. Rev.* **1948**, *73*, 679.
(31) Dong, R. Y. In *Encyclopedia of Spectroscopy and Spectrometry*; Academic Press: San Diego, CA, 1999, p 1568.